

ProtoMIL: Multiple Instance Learning with Prototypical Parts for Fine-Grained Interpretability

Dawid Rymarczyk^{1,2,*}, Aneta Kaczyńska^{1,*e}, Jarosław Kraus^{1,*e}, Adam Pardyl^{1,*e}, and Bartosz Zieliński^{1, 2,**}

¹Faculty of Mathematics and Computer Science, Jagiellonian University, 6 Łojasiewicza Street, 30-348 Kraków, Poland,

²Ardigen SA, 76 Podole Street, 30-394 Kraków, Poland,

*{dawid.rymarczyk, aneta.kaczyńska, jarosław.kraus, adam.pardyl}@student.uj.edu.pl

**{bartosz.zielinski}@uj.edu.pl

e denotes equal contribution

Abstract

Multiple Instance Learning (MIL) gains popularity in many real-life machine learning applications due to its weakly supervised nature. However, the corresponding effort on explaining MIL lags behind, and it is usually limited to presenting instances of a bag that are crucial for a particular prediction. In this paper, we fill this gap by introducing ProtoMIL, a novel self-explainable MIL method inspired by the case-based reasoning process that operates on visual prototypes. Thanks to incorporating prototypical features into objects description, ProtoMIL unprecedentedly joins the model accuracy and fine-grained interpretability, which we present with the experiments on five recognized MIL datasets.

1. Introduction

A typical supervised learning scenario assumes that each data point has a separate label. However, in many real-life applications, only one label is assigned to a set (bag) of instances due to the laborious and expensive process of instance labeling. This kind of problem, called Multiple Instance Learning (MIL) [13], assumes that an entire bag is described by only one label that corresponds to unspecified instances of this bag [16].

Multiple instance learning is recently observed in many real-life problems, like in the field of medical image analysis, where datasets usually contain weakly-labeled images of vast resolution [8, 30]. Notable, examples includ, but are not limited to: whole slide-image classification of biopsies

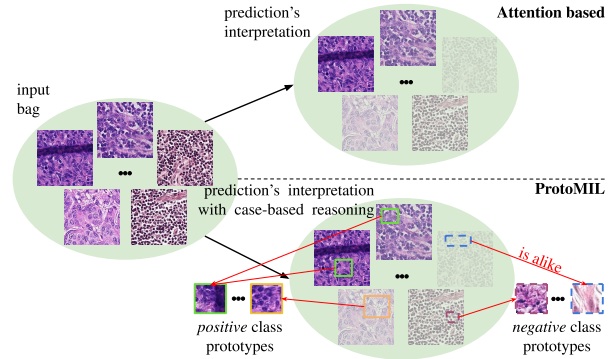


Figure 1: Comparison of predictions' interpretations for Attention-based MIL pooling (AbMILP) and ProtoMIL. In AbMILP, the most important instances obtain higher weights in weighted average (here presented as less transparent). ProtoMIL provides this information but additionally explains which parts of the instances are similar to prototypical parts corresponding to positive and negative classes. As a result, we obtain fine-grained interpretability of MIL model.

[6, 7, 21, 48], the diabetic retinopathy screening [31, 32], bacteria clones identification using microscopy images [5], or identify conformers responsible for molecule activity in drug design [43, 49].

In recent years, with the rapid development of deep learning, MIL is combined with many neural network-based models [15, 20, 25, 28, 35, 39, 40, 44, 45, 46]. Many of them embed all instances of the bag using a convolutional block of a deep network and then aggregate those embed-

dings. Moreover, some aggregation methods specify the most important instances that are presented to the user as prediction interpretation [20, 25, 28, 35, 40], as shown in the upper part of Figure 1. However, those methods usually only exhibit instances crucial for the prediction and do not indicate the cause of their importance. Naturally, there were attempts to further explain the MIL models [4, 5, 26], but overall, they usually introduce additional bias into the explanation [34] or require additional input [26].

To address the above shortcomings of MIL models, we introduce *Prototypical Multiple Instance Learning* (ProtoMIL). It builds on case-based reasoning, a type of explanation naturally used by humans to describe their thinking process [24]. More precisely, we divide each instance into patches and then quantify the similarities between those patches and a trainable set of positive and negative prototypical parts, as defined in [9]. Then, we apply an attention pooling operator to aggregate the similarities over instances and obtain bag-level representation that can be classified with an additional neural layer. This approach significantly differs from non-MIL approaches because it applies an aggregation layer and introduces a novel regularization technique that encourages the model to derive prototypes from the instances responsible for the positive label of a bag. The latter is a challenging problem because those instances are concealed and underrepresented. Lastly, the prototypical parts are pruned to obtain a compact characterization of the data classes. This results in a fine-grained interpretation of the prediction, as shown in Figure 1.

To show the effectiveness of our model, we conduct experiments on five datasets: MNIST Bags [20], Bisque breast Cancer [17], Colon Cancer [42], Retinopathy Screening (Messidor) [12], and Camelyon16 Breast Cancer [14]. The results we obtain are usually on par with the current state-of-the-art models. However, we strongly enhanced interpretation capabilities by describing the positive and negative classes with prototypical parts obtained with the training set. Our implementation of ProtoMIL is available at: *anonymized*.

The main contributions of this work are as follows:

- Introducing ProtoMIL model that substantially improves MIL models interpretability using case-based reasoning.
- Developing a training paradigm that generates prototypical parts also for the underrepresented instances responsible for the positive label of a bag.
- Defining prototypical parts pruning that removes confusing prototypes to increase its interpretability.

The paper is organized as follows. In Section 2, we present recent advancements in multiple instance learning and deep interpretable models. In Section 3, we define

the MIL paradigms, describe ProtoPNet, and introduce ProtoMIL. Finally, in Section 4, we present the results of conducted experiments and summarize the work in Section 5.

2. Related works

Our work relates to the field of Multiple Instance Learning (MIL) and eXplainable Artificial Intelligence (XAI), which we briefly describe in the following subsections.

2.1. Multiple instance learning

Before the deep learning era, models based on SVM, like MI-SVM [2], were used for MIL problems. However, currently, MIL is addressed with numerous deep models. One of them, Deep MIML [15], introduces a sub-concept layer that is learned and then pooled to obtain a bag representation. Another example is mi-Net [45], which pools predictions from single instances to derive a bag-level prediction. Other architectures adopted to MIL scenarios includes capsule networks [46], transformer [39] and graph neural networks [44]. Moreover, many works focus on the attention-based pooling operators, like AbMILP introduced in [20] that weights the instances embeddings to obtain a bag embedding. This idea was also extended by combining it with mi-Net [25], clustering similar instances [28], self-attention mechanism [35], and sharing classifier weights with pooling operator [40]. However, the above methods either do not contain an XAI component or only present the importance of the instances. Hence, our ProtoMIL is a step forward into the explainability of the MIL methods.

2.2. Explainable artificial intelligence

There are two types of eXplainable Artificial Intelligence (XAI) approaches, post hoc and self-explaining methods [3]. Among many *post hoc* techniques, one can distinguish saliency maps showing pixel importance [33, 37, 38, 41] or concept activation vectors representing internal network state with human-friendly concepts [10, 18, 22, 47]. They are easy to use since they do not require any changes in the model architecture. However, their explanations may be unfaithful and fragile [1]. Therefore *self-explainable* models were introduced like Prototypical Part Network [9] with a layer of prototypes representing the activation patterns. A similar approach for hierarchically organized prototypes is presented in [19] to classify objects at every level of a predefined taxonomy. Moreover, some works concentrate on transforming prototypes from the latent space to data space [27] or focus on sharing prototypical parts between classes and finding semantic similarities [36]. While others [29] build a decision tree with prototypical parts in the nodes or learn disease representative features within a dynamic area [23]. Nonetheless, to our best knowledge, no fine-grained self-explainable method, like ProtoMIL, exists for MIL problems.

3. Methods

In this section, we present ProtoMIL, a novel self-explainable MIL inspired by the case-based reasoning process (see Section 3.3). However, to make this paper self-contained, we first recall definitions of MIL and Attention-based MIL pooling [20] in Sections 3.1, and then we briefly describe ProtoPNet architecture in Sections 3.2.

3.1. Multiple instance learning

Lets denote a single instance as x_i and its corresponding label as $y_i \in \{0, 1\}$. Bear in mind that for each instance, such a label exists but is not accessible during training. Given a bag of instances $X = \{x_1, \dots, x_k\}$, MIL aims to predict the label of the entire bag defined as:

$$y = \begin{cases} 0, & \text{iff } \sum_{i=1}^k y_i = 0, \\ 1, & \text{otherwise.} \end{cases} \quad (1)$$

The classification of a bag of instances consists of three steps: (i) transforming instances using a function f , (ii) combining transformed instances using symmetric (permutation-invariant) function σ , (iii) and transforming combined instances using function g . The choice of functions f , σ and g varies between approaches, and σ function is referred as MIL pooling.

Attention-based MIL pooling (AbMILP). AbMILP [20] is an embedding-based MIL approach. It starts by mapping instances from a given bag X into a low-dimensional space to obtain their embeddings $H = \{h_1, \dots, h_k\}$, $h_i \in \mathbb{R}^M$. Then, it performs the following MIL pooling to obtain a representation of the whole bag:

$$h_{\text{bag}} = \sum_{i=1}^k a_i h_i \quad (2)$$

where:

$$a_i = \frac{\exp\{\mathbf{w}^T (\tanh(\mathbf{V}h_i^T) \odot \text{sigm}(\mathbf{U}h_i^T))\}}{\sum_{j=1}^k \exp\{\mathbf{w}^T (\tanh(\mathbf{V}h_j^T) \odot \text{sigm}(\mathbf{U}h_j^T))\}}, \quad (3)$$

where $\mathbf{w} \in \mathbb{R}^{L \times 1}$, $\mathbf{V} \in \mathbb{R}^{L \times M}$, and $\mathbf{U} \in \mathbb{R}^{L \times M}$ are parameters, \tanh is the hyperbolic tangent, sigm is the sigmoid non-linearity and \odot is an element-wise multiplication. Note that weights a_i sum up to 1, and thus the formula is invariant to the size of the bag.

3.2. ProtoPNet

ProtoPNet [9] mimics human-like reasoning by incorporating prototypes of each class in its architecture and

making a prediction based on the presence of some class-specific prototypical parts in the input image. It consists of a regular convolutional neural network f_{conv} followed by a prototype layer f_{proto} and a fully connected layer g . Prototype layer stores a fixed number of learnable prototypes for every class. Each prototype can be understood as a latent representation of some prototypical part of a certain image from a given class. The input image is forwarded through convolutional layers to extract useful features. Next, the prototype layer computes similarity scores between each prototype and image's patches. This results in an activation map of similarity scores with values indicating how strong a prototypical part is present in the image. The activation map is then reduced to a single similarity score for each prototype using global max pooling. The higher the similarity score, the stronger representation of a given prototypical part in *some* patch of the input image. In the last step, a pooled vector of similarity scores is forwarded through the last layer to make the final prediction.

3.3. ProtoMIL

To incorporate an additional level of interpretability into the MIL scenario, we combined ProtoPNet with Attention-based MIL pooling (AbMILP). We opt for using AbMILP due to its high performance and interpretability. However, it could be easily replaced by any other pooling operator.

ProtoMIL, presented in Figure 2, consists of four modules: convolutional network f_{conv} , prototype layer f_{proto} , attention pooling a and fully connected last layer g . Convolutional and prototype layers process single instances, whereas attention pooling and the last layer work on a bag's representation. More precisely, given a bag of instances $X = \{x_1, \dots, x_k\}$, each instance is forwarded through convolutional layers to obtain low-dimensional embeddings $F = \{f_{\text{conv}}(x_1), \dots, f_{\text{conv}}(x_k)\}$. Then, for each embedding $f_{\text{conv}}(x_i)$, a vector h_i of similarity scores between the given embedding and all prototypes is computed by the prototype layer, the same way as described in Section 3.2. This results in a bag of similarity scores vectors $H = \{h_1, \dots, h_k\}$ on which the attention pooling is applied to achieve a single similarity score vector h_{bag} representing the entire bag of instances. Obtained representation is then forwarded through the last layer that returns the predicted bag label.

As the convolutional layer f_{conv} , we use convolutional block from ResNet-18 and follow it by two additional 1×1 convolutions. We use ReLU as the activation function for all convolutional layers except the last layer, for which we use the sigmoid activation function. Prototype layer stores prototypes that are shared across all bags, while the attention layer implements AbMILP. The last layer is used to classify the entire bag. Weights between similarity scores of prototypes corresponding class logit are initialized with 1, while

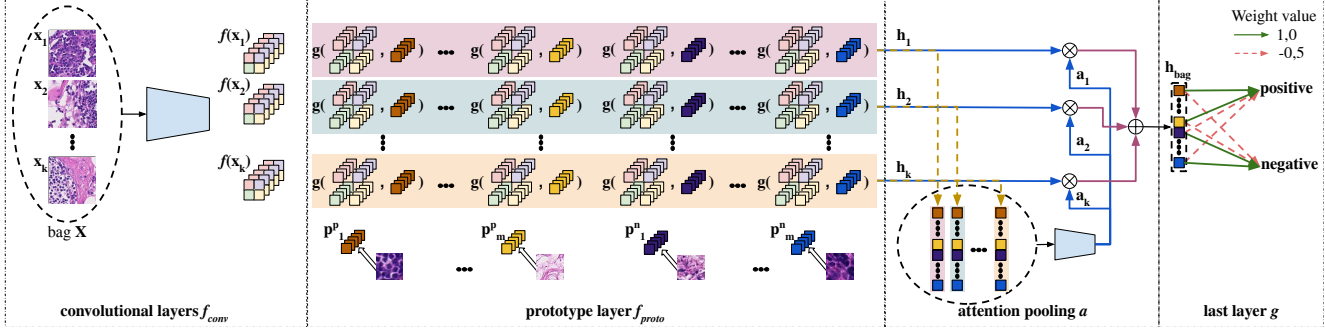


Figure 2: The architecture of the ProtoMIL consists of a convolutional layer f_{conv} that derives embeddings for each instance of a bag. Then, it calculates similarities between instances’ representations and prototypes from layer f_{proto} . The similarities are aggregated using the attention pooling a . The resulting bag representation is classified using the last layer g . Notice that particular colors in vectors \mathbf{h}_i and \mathbf{h}_{bag} correspond to prototypes’ similarities (brown and yellow for positive class, and dark and bright blue for negative class).

other connections are set to -0.5 as in [9]. Together with the specific training procedure, such initialization results in a positive reasoning process (we rather say “this looks like that” instead of saying “this does not look like that”).

Prototypes projection. Prototypes projection is an important step in the training procedure that visualizes the prototypes as training image patches. More specifically, it replaces every learned prototype with the representation of the nearest training patch from the bag with the same label as the prototype’s class. For prototype \mathbf{p}_j^c of class c (negative or positive), it can be expressed by the following formula:

$$\mathbf{p}_j^c \leftarrow \arg \min_{\mathbf{z} \in Z} \|\mathbf{z} - \mathbf{p}_j^c\|_2, \quad (4)$$

where $Z = \{\tilde{\mathbf{z}} \in Z_{x_i} | x_i \in X \wedge y = c\}$, X and y denote a bag together with its label, and Z_{x_i} denotes representations of the x_i patches.

Regularization. As we already mentioned in Section 1, the instances responsible for the positive label of a bag are concealed and underrepresented. As a result, training ProtoMIL without additional regularizations can result in a prototype layer containing only negative prototypes. Hence, to prevent this, we introduce a novel regularization technique that encourages the model to derive prototypes from the instances responsible for the positive label of a bag.

For this purpose, we introduce the loss function, constructed from three components:

$$\mathcal{L}_{CE}(\tilde{y}, y) + \lambda_1 \mathcal{L}_{Clst} + \lambda_2 \mathcal{L}_{Sep} \quad (5)$$

where \tilde{y} and y denotes respectively the predicted and ground truth label of bag $X = \{x_1, \dots, x_k\}$, \mathcal{L}_{CE} corresponds to cross-entropy loss, while \mathcal{L}_{Clst} and \mathcal{L}_{Sep} are ap-

propriately modified cluster and separation losses from [9]:

$$\mathcal{L}_{Clst} = \frac{1}{k} \sum_{i=1}^k a_i \min_{j: \mathbf{p}_j^y \in P_y} \min_{\mathbf{z} \in Z_{x_i}} \|\mathbf{z} - \mathbf{p}_j^y\|_2^2, \quad (6)$$

$$\mathcal{L}_{Sep} = -\frac{1}{k} \sum_{i=1}^k a_i \min_{j: \mathbf{p}_j^y \notin P_y} \min_{\mathbf{z} \in Z_{x_i}} \|\mathbf{z} - \mathbf{p}_j^y\|_2^2, \quad (7)$$

where P_y is a set of prototypes for a data class consisted of prototypical parts \mathbf{p}_j^y ($y = n$ for a negative class and $y = p$ for a positive one).

Intuitively, cluster cost with attention weights encourages the model to create positive prototypes for instances responsible for the positive label of a bag because those instances have the highest values a_i . On the other hand, separation cost with attention weights encourages negative prototypes to keep away from those instances. Without this modification, instances responsible for the positive label would have to be known during training to use the prototype approach.

Pruning. During the prototype projection, every prototype is replaced with the representation of the nearest training patch from the bag with the same label. Generally, the representations of the nearest training patches correspond to the same label. However, in some cases, the nearest patches of a prototype correspond to more than one class. It is especially problematic in highly unbalanced datasets, frequently occurring in MIL tasks. To remove such misleading prototypes, we extend the prototype pruning algorithm from [9] to work in the MIL scenario. More precisely, we find k -nearest training patches for each prototype \mathbf{p}_i^c belonging to class c . If out of those k patches less than r belong to bags labeled with class c , we assume that this prototype is not

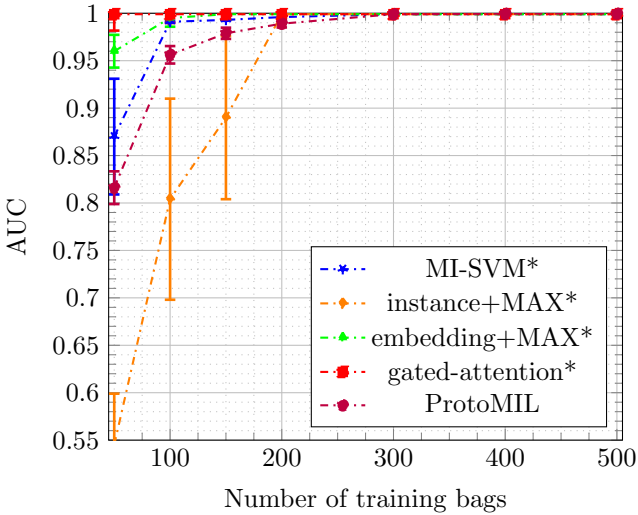


Figure 3: Results for ProtoMIL and baseline MIL approaches on the MNIST Bags dataset depending on the number of training bags (x axis) using the AUC metric (y axis). One can observe that ProtoMIL achieves state-of-the-art results with a larger number of samples.



Figure 4: Sample positive and negative prototypes of ProtoMIL trained on the MNIST Bags dataset. Notice that the positive prototypes correspond to parts of “9” while the negative prototypes contain parts of the other digits (like “8” or “4”). It is expected because a bag is considered positive if it contains at least one image of “9”.

determinant and remove it. Moreover, in contrast to [9], we automatically select r to remove up to $l\%$ of prototypes (l and k are selected so that both classes still contain prototypes, and the drop in training accuracy is minimal). Finally, we fine-tuned attention and the final layers to compensate for the prototype removal.

4. Experiments

We test our ProtoMIL approach on five datasets. All models are trained from scratch in three steps: (i) *warmup* phase with training all layers except the last one, (ii) prototype projection, (iii) and fine-tuning with fixed f_{conv} and f_{proto} . Phases (ii) and (iii) are repeated several times to find the most optimal set of prototypes. All trainings use Adam optimizer for all layers with $\beta_1 = 0.99$, $\beta_2 = 0.999$, weight decay 0.001, and batch size 1. Additionally, we use an exponential learning rate scheduler for the *warmup* phase and

a step scheduler for prototype training. All results are reported as an average of all runs with a standard error of the mean. In the subsequent subsections, we describe experiment details and results for each of the dataset.

4.1. MNIST Bags

Experiment details. We start our experiments with the MNIST dataset, for which we generate the bags like proposed in [20]. Namely, a single bag contains grayscale images randomly sampled from the MNIST dataset. The bags’ sizes are chosen using a normal distribution with a mean of 100 and a standard deviation of 20. A bag is considered positive if it contains at least one image labeled as “9”. There are equal numbers of positive and negative bags. Notice that even though such dataset is class-balanced, it contains only 5% of images labeled as “9” (10% instances in the positive bags). We test ProtoMIL for different size of dataset (50, 100, 200, 300, 400, 500 bags). Every experiment is run with random 10-fold cross-validation and repeated five times with a different seed to obtain mean AUC as the evaluation metric. We train a model for 30, 20, and 10 epochs for warmup, fine-tuning, and end-to-end training, respectively. The number of prototypes per class is set to 10, with prototype size $64 \times 2 \times 2$ (determined experimentally).

Results. We compare our model to baseline MIL pooling methods from [20]. As shown, our ProtoMIL approach requires slightly more samples to achieve AUC scores competitive to the regular models (Figure 3). However, as presented in Figure 5a, it increases model interpretability by finding distinct parts of images and match them with intuitive positive and negative prototypes (see Figure 4).

4.2. Bisque and Colon Cancer datasets

Experiment details. Secondly, we experiment on two histological datasets: Colon Cancer and Bisque breast cancer. The former contains 100 H&E images with 22,444 manually annotated nuclei of four different types: epithelial, inflammatory, fibroblast, and miscellaneous. To create bags of instances, we extract 27×27 nucleus-centered patches from each image, and the goal is to detect if the bag contains one or more epithelial cells, as colon cancer originates from them. On the other hand, the Bisque dataset consists of 58 H&E breast histology images of size 896×768 , out of which 32 are benign, and 26 are malignant (contain at least one cancer cell). Each image is divided into 32×32 patches, resulting in 672 patches per image. Patches with at least 75% of the white pixels are discarded, resulting in 58 bags of various sizes.

We apply extensive data augmentation for both datasets, including random rotations, horizontal and vertical flipping, random staining augmentation, staining normalization, and instance normalization. We use ResNet-18 convolutional

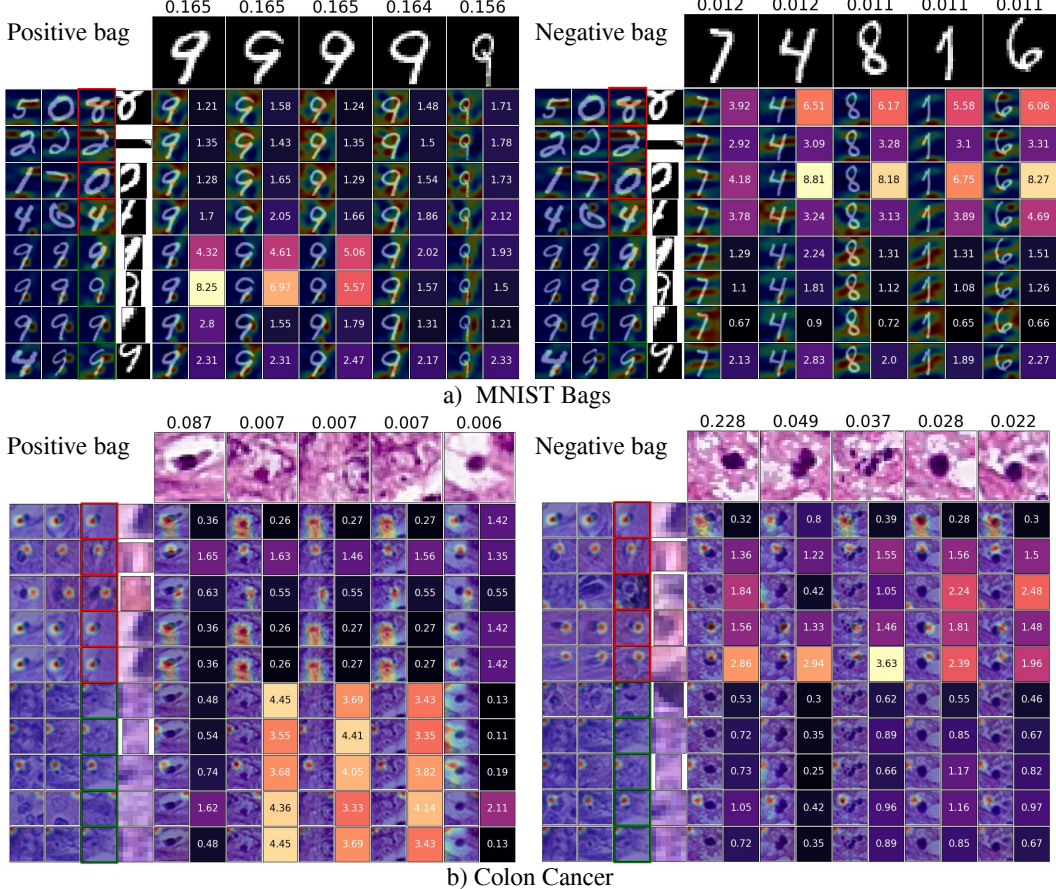


Figure 5: Similarity scores between five crucial instances of a bag (columns) and eight or ten prototypical parts (rows) for a positive and negative bag (left and right side, respectively) from the MNIST Bags (a) and Colon Cancer datasets (b). Each prototypical part is represented by a part of image and three nearest training patches, and each instance is represented by the image and the value of attention weight a_i . Moreover, each cell contains a similarity score and a heatmap corresponding to prototype activation. One can observe that instances of a negative bag usually activate negative prototypes (four upper prototypes in red brackets), while the instances of positive bags mostly activate positive prototypes (four bottom prototypes in green brackets).

| METHOD | BISQUE | | COLON CANCER | |
|-----------------|------------------------------------|-------------------------------------|------------------------------------|-------------------------------------|
| | ACCURACY | AUC | ACCURACY | AUC |
| INSTANCE+MAX* | 61.4% \pm 2.0% | 0.612 \pm 0.026 | 84.2% \pm 2.1% | 0.914 \pm 0.010 |
| INSTANCE+MEAN* | 67.2% \pm 2.6% | 0.719 \pm 0.019 | 77.2% \pm 1.2% | 0.866 \pm 0.008 |
| EMBEDDING+MAX* | 60.7% \pm 1.5% | 0.650 \pm 0.013 | 82.4% \pm 1.5% | 0.918 \pm 0.010 |
| EMBEDDING+MEAN* | 74.1% \pm 2.3% | 0.796 \pm 0.012 | 86.0% \pm 1.4% | 0.940 \pm 0.010 |
| ABMILP* | 71.7% \pm 2.7% | 0.856 \pm 0.022 | 88.4% \pm 1.4% | 0.973 \pm 0.007 |
| SA-ABMILP** | 75.1% \pm 2.4% | 0.862 \pm 0.022 | 90.8% \pm 1.3% | 0.981 \pm 0.007 |
| PROTOMIL (OUR) | 76.7% \pm 2.2% | 0.886 \pm 0.033 | 81.3% \pm 1.9% | 0.932 \pm 0.014 |

Table 1: Results for small histological datasets. ProtoMIL significantly outperforms baseline methods on the Bisque dataset. However, it achieves slightly worse results for the Colon Cancer dataset, probably due to its small size. Notice that values for comparison indicated with “*” and “**” comes from [20] and [35], respectively.

| METHOD | ACCURACY | F-SCORE |
|----------------|--------------|-------------|
| MI-SVM* | 54.5% | 0.70 |
| MI-SVM* | 54.5% | 0.71 |
| EMDD* | 55.1% | 0.69 |
| CITATION k-NN* | 62.8% | 0.69 |
| MILBOOST* | 64.1% | 0.66 |
| MI-GRAPH* | 72.5% | 0.75 |
| MIL-GNN-ATT* | 72.9% | 0.75 |
| MIL-GNN-DP* | 74.2% | 0.77 |
| ABMILP** | 74.5% | 0.74 |
| SA-ABMILP** | 75.2% | 0.76 |
| LSA-ABMILP** | 76.3% | 0.77 |
| PROTOMIL (OUR) | 70.0% | 0.75 |

Table 2: Results for the Messidor dataset show that in terms of F-score, our ProtoMIL method is comparable with methods based on attention (AbMILP) or graph convolutions (MIL-GNN-ATT). Notice that values for comparison marked with “*” and “**” are taken from [44] and [35], respectively.

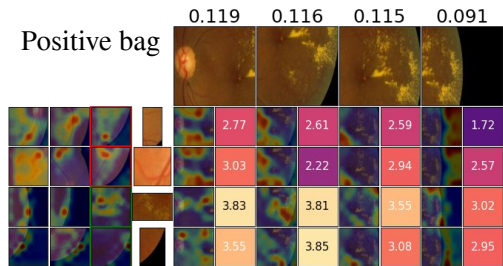


Figure 6: Similarity scores between four crucial instances of a bag (columns) and four prototypical parts (rows) for a positive bag from the Messidor dataset. One can observe that ProtoMIL focuses on the disease factors, which are the brightest yellow spots on the image. Moreover, both positive and negative prototypes are activated since the retina with pathological changes still shows healthy features, such as veins. Please refer to Figure 5 for a detailed description of the visualization.

parts with the first layer modified to 3×3 convolution with stride 1 to match the size of smaller instances. We set the number of prototypes per class to 10 with a size of $128 \times 2 \times 2$. Warmup, fine-tuning, and end-to-end training take 60, 20, and 20 epochs, respectively. 10-fold cross-validation with 1 validation fold and 1 test fold is repeated 5 times.

Results. Table 1 presents our results compared to both traditional and attention-based MIL models. On the Bisque dataset, our model significantly outperforms all baseline models. However, due to the small size of the Colon Cancer

| METHOD | ACCURACY | AUC |
|----------------|---------------|--------------|
| MEAN-POOLING* | 79.84% | 0.762 |
| MAX-POOLING* | 82.95% | 0.864 |
| MILRNN* | 80.62% | 0.807 |
| ABMILP* | 84.50% | 0.865 |
| DSMIL* | 86.82% | 0.894 |
| CLAM-SB** | 87.60% | 0.881 |
| CLAM-MB** | 83.72% | 0.868 |
| TRANSMIL** | 88.37% | 0.931 |
| PROTOMIL (our) | 87.29% | 0.935 |

Table 3: Our ProtoMIL achieves state-of-the-art results on the Camelyon16 dataset in terms of AUC metric, surpassing even the transformer-based architecture. Notice that values for comparison marked with “*” and “***” are taken from [25] and [39], respectively.

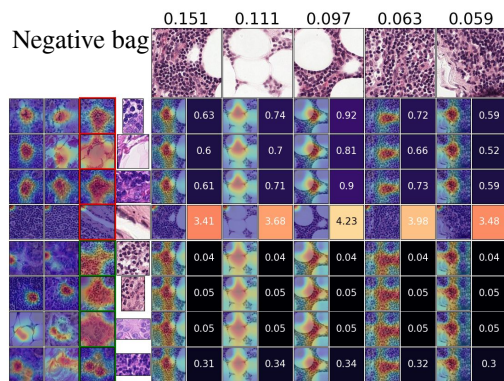


Figure 7: Similarity scores between five crucial instances of a bag (columns) and eight prototypical parts (rows) for a negative bag from the Camelyon16 dataset. One can observe that ProtoMIL strongly activates only one prototype and focuses mainly on nuclei when analyzing the healthy parts of the tissue. Please refer to Figure 5 for a detailed description of the visualization.

dataset, ProtoMIL overfits, resulting in poorer AUC than attention-based models. Nevertheless, in both cases, ProtoMIL provides finer explanations than all baseline models (see Figure 5b and Supplementary Materials).

4.3. Messidor dataset

Experiment details. The Messidor dataset contains 1200 retinal images: 654 with a positive label (diabetic retinopathy) and 546 with a negative one. To create bags of instances, we crop overlapping patches of size 224×224 from each of 700×700 images, and patches with more than 70% black pixels are dropped as in [44]. Additionally, we apply extensive data augmentation, including random rotations, horizontal and vertical flipping, Gaussian noise, and

| DATASET | BEFORE PRUNING | | | AFTER PRUNING | | |
|----------------|----------------|-------------------|-------------------|------------------|------------------|-------------------|
| | PROTOTYPES | ACCURACY | AUC | PROTOTYPES | ACCURACY | AUC |
| MNIST BAGS 500 | 20 \pm 0 | 99.2% \pm 0.1% | 0.999 \pm 0.001 | 14.12 \pm 0.28 | 99.2% \pm 0.1% | 0.999 \pm 0.001 |
| BISQUE | 20 \pm 0 | 76.7% \pm 2.2% | 0.886 \pm 0.033 | 13.68 \pm 0.25 | 73.0% \pm 2.4% | 0.867 \pm 0.022 |
| COLON CANCER | 20 \pm 0 | 81.3% \pm 1.9% | 0.932 \pm 0.014 | 15.69 \pm 0.34 | 81.8% \pm 2.4% | 0.880 \pm 0.022 |
| MESSIDOR | 20 \pm 0 | 70.0% \pm 0.9% | 0.692 \pm 0.012 | 16.70 \pm 1.86 | 64.7% \pm 1.3% | 0.717 \pm 0.013 |
| CAMELYON16 | 10 \pm 0 | 87.3% \pm 1.2 % | 0.935 \pm 0.007 | 6.40 \pm 0.24 | 85.9% \pm 1.5% | 0.937 \pm 0.007 |

Table 4: The influence of ProtoMIL pruning on the accuracy and AUC score. One can notice that even though the pruning removes around 30% of the prototypes, it usually does not noticeably decrease the AUC and accuracy of the model.

patch normalization. We use ResNet-18 convolutional layers learned from scratch with 10 prototypes per class and prototype size of $1 \times 1 \times 128$. Warmup, fine-tuning, and end-to-end training take 30, 20, and 10 epochs, respectively. We perform 10 fold cross-validation repeated two times as in [44].

Results. Results of ProtoMIL in the case of F-score are comparable with the ones achieved in [44] and [35] (see Table 2). However, the accuracy is significantly lower, most possibly due to the data class imbalance. Nevertheless, our model provides a fine-grained interpretation of its decision, as presented in Figure 6.

4.4. Camelyon16 dataset

Experiment details. The Camelyon16 dataset [14] consists of 399 whole-slide images of breast cancer samples, each labeled as *normal* or *tumor*. We create MIL bags by dividing each slide $20x$ resolution image into 224×224 patches, rejecting patches that contain more than 70% of background. This results in 399 bags with a mean of 8871 patches and a standard deviation of 6175. Moreover, 20 largest bags are truncated to 20000 random patches to fit into the memory of a GPU. The positive patches are again highly imbalanced, as only less than 10% of patches contain tumor tissue.

Due to the size of the dataset, we preprocess all samples using a ResNet-18 without two last layers, pre-trained on various histopathological images using self-supervised learning from [11]. The resulting embeddings are fed into our model to replace the feature backbone net. ProtoMIL is trained for 50, 40, and 10 epochs in warmup, fine-tuning, and end-to-end training, respectively. The number of prototypes per class is limited to 5 with no data augmentation. The experiments are repeated 5 times with the original train-test split.

Results. We compare ProtoMIL to other state-of-the-art MIL techniques, including both traditional mean and max MIL pooling, RNN, attention-based MIL pooling, and transformer-based MIL pooling [39]. ProtoMIL performs

on par in terms of accuracy and slightly outperforms other models on AUC metric (Table 3) while providing a better understanding of its decision process, as presented in Figure 7 and Supplementary Materials.

4.5. Pruning

Experiment details. We run prototype pruning experiments on MNIST Bags (with 500 training bags), Bisque, Colon Cancer, Messidor, and Camelyon16 datasets. For all datasets, we use the model trained in the previously described experiments. As pruning parameters, we use $k = 6$ and $l = 40\%$ and fine-tuned for 20 epochs.

Results. The accuracy and AUC in respect to the number of prototypes before and after pruning are presented in Table 4. For all datasets, the number of prototypes after pruning has decreased around 30% on average. However, it does not result in a noticeable decrease in accuracy or AUC, except for Colon Cancer, where we observe a significant drop in AUC. Most probably, it is caused by the high visual resemblance of nuclei patches (especially between *epithelial* and *miscellaneous*) that after prototype projection may be very close to each other in the latent space. Interestingly, in the case of the Messidor dataset, AUC has even increased by 0.025 after pruning.

5. Discussion and conclusions

In this work, we introduce Prototypical Multiple Instance Learning (ProtoMIL), which incorporates a case-based reasoning process into the attention-based MIL setup. In contrast to existing methods, except explaining its decision globally by presenting the crucial instances, ProtoMIL provides a fine-grained interpretation using trainable positive and negative prototypical parts. The experiments on five datasets confirm that introducing fine-grained interpretability does not reduce the model’s effectiveness, which is still on par with the current state-of-the-art methodology. Moreover, the results can be presented to the user with a new visualization technique that we introduced. Finally, we define pruning operation, which reduces many prototypes

without loss in accuracy and AUC score, making the class description easier and faster to understand by humans.

The experiments show that ProtoMIL can be applied to such challenging real-life problems as medical imaging. Therefore, in future works, we plan to generalize our method to multi-label scenarios and different data types, like graphs.

References

- [1] Julius Adebayo, Justin Gilmer, Michael Muelly, Ian Goodfellow, Moritz Hardt, and Been Kim. Sanity checks for saliency maps. In *Advances in neural information processing systems*, pages 9505–9515, 2018.
- [2] Stuart Andrews, Ioannis Tsochantaridis, and Thomas Hofmann. Support vector machines for multiple-instance learning. In *Advances in neural information processing systems*, volume 2, page 7, 2002.
- [3] Vijay Arya, Rachel KE Bellamy, Pin-Yu Chen, Amit Dhurandhar, Michael Hind, Samuel C Hoffman, Stephanie Houde, Q Vera Liao, Ronny Luss, Aleksandra Mojsilović, et al. One explanation does not fit all: A toolkit and taxonomy of ai explainability techniques. *arXiv preprint arXiv:1909.03012*, 2019.
- [4] Alina Jade Barnett, Fides Regina Schwartz, Chaofan Tao, Chaofan Chen, Yinhao Ren, Joseph Y Lo, and Cynthia Rudin. Iaia-bl: A case-based interpretable deep learning model for classification of mass lesions in digital mammography. *arXiv preprint arXiv:2103.12308*, 2021.
- [5] Adriana Borowa, Dawid Rymarczyk, Dorota Ochońska, Monika Brzyczy-Włoch, and Bartosz Zieliński. Classifying bacteria clones using attention-based deep multiple instance learning interpreted by persistence homology. In *International joint conference on neural networks*, 2021.
- [6] Gabriele Campanella, Matthew G Hanna, Luke Geneslaw, Allen Miraflor, Vitor Werneck Krauss Silva, Klaus J Busam, Edi Brogi, Victor E Reuter, David S Klimstra, and Thomas J Fuchs. Clinical-grade computational pathology using weakly supervised deep learning on whole slide images. *Nature medicine*, 25(8):1301–1309, 2019.
- [7] Gabriele Campanella, Vitor Werneck Krauss Silva, and Thomas J Fuchs. Terabyte-scale deep multiple instance learning for classification and localization in pathology. *arXiv preprint arXiv:1805.06983*, 2018.
- [8] Marc-André Carbonneau, Veronika Cheplygina, Eric Granger, and Ghyslain Gagnon. Multiple instance learning: A survey of problem characteristics and applications. *Pattern Recognition*, 77:329–353, 2018.
- [9] Chaofan Chen, Oscar Li, Chaofan Tao, Alina Jade Barnett, Jonathan Su, and Cynthia Rudin. This looks like that: deep learning for interpretable image recognition. *arXiv preprint arXiv:1806.10574*, 2018.
- [10] Zhi Chen, Yijie Bei, and Cynthia Rudin. Concept whitening for interpretable image recognition. *Nature Machine Intelligence*, 2(12):772–782, 2020.
- [11] Ozan Ciga, Anne L Martel, and Tony Xu. Self supervised contrastive learning for digital histopathology. *arXiv preprint arXiv:2011.13971*, 2020.
- [12] Etienne Decencière, Xiwei Zhang, Guy Cazuguel, Bruno Lay, Béatrice Cochener, Caroline Trone, Philippe Gain, Richard Ordonez, Pascale Massin, Ali Erginay, et al. Feedback on a publicly distributed image database: the messidor database. *Image Analysis & Stereology*, 33(3):231–234, 2014.
- [13] Thomas G Dietterich, Richard H Lathrop, and Tomás Lozano-Pérez. Solving the multiple instance problem with axis-parallel rectangles. *Artificial intelligence*, 89(1-2):31–71, 1997.
- [14] Babak Ehteshami Bejnordi, Mitko Veta, Paul Johannes van Diest, Bram van Ginneken, Nico Karssemeijer, Geert Litjens, Jeroen A. W. M. van der Laak, , and the CAMELYON16 Consortium. Diagnostic Assessment of Deep Learning Algorithms for Detection of Lymph Node Metastases in Women With Breast Cancer. *JAMA*, 318(22):2199–2210, 12 2017.
- [15] Ji Feng and Zhi-Hua Zhou. Deep miml network. In *Proceedings of the AAAI Conference on Artificial Intelligence*, volume 31, 2017.
- [16] James Foulds and Eibe Frank. A review of multi-instance learning assumptions. *The Knowledge Engineering Review*, 25(1):1–25, 2010.
- [17] Elisa Drelie Gelasca, Jiyun Byun, Boguslaw Obara, and BS Manjunath. Evaluation and benchmark for biological image segmentation. In *2008 15th IEEE International Conference on Image Processing*, pages 1816–1819. IEEE, 2008.
- [18] Amirata Ghorbani, James Wexler, James Y Zou, and Been Kim. Towards automatic concept-based explanations. In *Advances in neural information processing systems*, pages 9277–9286, 2019.
- [19] Peter Hase, Chaofan Chen, Oscar Li, and Cynthia Rudin. Interpretable image recognition with hierarchical prototypes. In *Proceedings of the AAAI Conference on Human Computation and Crowdsourcing*, volume 7, pages 32–40, 2019.
- [20] Maximilian Ilse, Jakub Tomczak, and Max Welling. Attention-based deep multiple instance learning. In *International conference on machine learning*, pages 2127–2136. PMLR, 2018.
- [21] Maximilian Ilse, Jakub M Tomczak, and Max Welling. Deep multiple instance learning for digital histopathology. In *Handbook of Medical Image Computing and Computer Assisted Intervention*, pages 521–546. Elsevier, 2020.
- [22] Been Kim, Martin Wattenberg, Justin Gilmer, Carrie Cai, James Wexler, Fernanda Viegas, et al. Interpretability beyond feature attribution: Quantitative testing with concept activation vectors (tcav). In *International conference on machine learning*, pages 2668–2677. PMLR, 2018.
- [23] Eunji Kim, Siwon Kim, Minji Seo, and Sungroh Yoon. Xprononet: Diagnosis in chest radiography with global and local explanations. In *Proceedings of the IEEE/CVF Conference on Computer Vision and Pattern Recognition*, pages 15719–15728, 2021.
- [24] Janet Kolodner. *Case-based reasoning*. Morgan Kaufmann, 2014.
- [25] Bin Li, Yin Li, and Kevin W Eliceiri. Dual-stream multiple instance learning network for whole slide image classifica-

tion with self-supervised contrastive learning. In *Proceedings of the IEEE/CVF Conference on Computer Vision and Pattern Recognition*, pages 14318–14328, 2021.

[26] Guangli Li, Chuanxiu Li, Guangting Wu, Donghong Ji, and Hongbing Zhang. Multi-view attention-guided multiple instance detection network for interpretable breast cancer histopathological image diagnosis. *IEEE Access*, 2021.

[27] Oscar Li, Hao Liu, Chaofan Chen, and Cynthia Rudin. Deep learning for case-based reasoning through prototypes: A neural network that explains its predictions. In *Proceedings of the AAAI Conference on Artificial Intelligence*, volume 32, 2018.

[28] Ming Y Lu, Drew FK Williamson, Tiffany Y Chen, Richard J Chen, Matteo Barbieri, and Faisal Mahmood. Data-efficient and weakly supervised computational pathology on whole-slide images. *Nature Biomedical Engineering*, 5(6):555–570, 2021.

[29] Meike Nauta, Ron van Bree, and Christin Seifert. Neural prototype trees for interpretable fine-grained image recognition. In *Proceedings of the IEEE/CVF Conference on Computer Vision and Pattern Recognition*, pages 14933–14943, 2021.

[30] Gwenolé Quellec, Guy Cazuguel, Béatrice Cochener, and Mathieu Lamard. Multiple-instance learning for medical image and video analysis. *IEEE reviews in biomedical engineering*, 10:213–234, 2017.

[31] Gwenolé Quellec, Mathieu Lamard, Michael D Abràmoff, Etienne Decencière, Bruno Lay, Ali Erginay, Béatrice Cochener, and Guy Cazuguel. A multiple-instance learning framework for diabetic retinopathy screening. *Medical image analysis*, 16(6):1228–1240, 2012.

[32] Priya Rani, Rajkumar Elagiri Ramalingam, Kumar T Rajamani, Melih Kandemir, and Digvijay Singh. Multiple instance learning: Robust validation on retinopathy of prematurity. *Int J Ctrl Theory Appl*, 9:451–459, 2016.

[33] Sylvestre-Alvise Rebuffi, Ruth Fong, Xu Ji, and Andrea Vedaldi. There and back again: Revisiting backpropagation saliency methods. In *Proceedings of the IEEE/CVF Conference on Computer Vision and Pattern Recognition*, pages 8839–8848, 2020.

[34] Cynthia Rudin. Stop explaining black box machine learning models for high stakes decisions and use interpretable models instead. *Nature Machine Intelligence*, 1(5):206–215, 2019.

[35] Dawid Rymarczyk, Adriana Borowa, Jacek Tabor, and Bartosz Zieliński. Kernel self-attention for weakly-supervised image classification using deep multiple instance learning. In *Proceedings of the IEEE/CVF Winter Conference on Applications of Computer Vision*, pages 1721–1730, 2021.

[36] Dawid Rymarczyk, Łukasz Struski, Jacek Tabor, and Bartosz Zieliński. Protoshare: Prototype sharing for interpretable image classification and similarity discovery. In *Proceedings of the 27th ACM SIGKDD Conference on Knowledge Discovery and Data Mining (KDD '21)*, 2021.

[37] Ramprasaath R Selvaraju, Michael Cogswell, Abhishek Das, Ramakrishna Vedantam, Devi Parikh, and Dhruv Batra. Grad-cam: Visual explanations from deep networks via gradient-based localization. In *Proceedings of the IEEE/CVF International Conference on Computer Vision*, pages 618–626, 2017.

[38] Ramprasaath R Selvaraju, Stefan Lee, Yilin Shen, Hongxia Jin, Shalini Ghosh, Larry Heck, Dhruv Batra, and Devi Parikh. Taking a hint: Leveraging explanations to make vision and language models more grounded. In *Proceedings of the IEEE/CVF International Conference on Computer Vision*, pages 2591–2600, 2019.

[39] Zhuchen Shao, Hao Bian, Yang Chen, Yifeng Wang, Jian Zhang, Xiangyang Ji, and Yongbing Zhang. Transmil: Transformer based correlated multiple instance learning for whole slide image classification. *arXiv preprint arXiv:2106.00908*, 2021.

[40] Xiaoshuang Shi, Fuyong Xing, Yuanpu Xie, Zizhao Zhang, Lei Cui, and Lin Yang. Loss-based attention for deep multiple instance learning. In *Proceedings of the AAAI Conference on Artificial Intelligence*, volume 34, pages 5742–5749, 2020.

[41] Karen Simonyan, Andrea Vedaldi, and Andrew Zisserman. Deep inside convolutional networks: Visualising image classification models and saliency maps. *arXiv:1312.6034*, 2013.

[42] Korsuk Sirinukunwattana, Shan E Ahmed Raza, Yee-Wah Tsang, David RJ Snead, Ian A Cree, and Nasir M Rajpoot. Locality sensitive deep learning for detection and classification of nuclei in routine colon cancer histology images. *IEEE transactions on medical imaging*, 35(5):1196–1206, 2016.

[43] Christoph Straehle, Melih Kandemir, Ullrich Koethe, and Fred A Hamprecht. Multiple instance learning with response-optimized random forests. In *2014 22nd International Conference on Pattern Recognition*, pages 3768–3773. IEEE, 2014.

[44] Ming Tu, Jing Huang, Xiaodong He, and Bowen Zhou. Multiple instance learning with graph neural networks. *arXiv preprint arXiv:1906.04881*, 2019.

[45] Xinggang Wang, Yongluan Yan, Peng Tang, Xiang Bai, and Wenyu Liu. Revisiting multiple instance neural networks. *Pattern Recognition*, 74:15–24, 2018.

[46] Yongluan Yan, Xinggang Wang, Xiaojie Guo, Jiemin Fang, Wenyu Liu, and Junzhou Huang. Deep multi-instance learning with dynamic pooling. In *Asian Conference on Machine Learning*, pages 662–677. PMLR, 2018.

[47] Chih-Kuan Yeh, Been Kim, Sercan O Arik, Chun-Liang Li, Tomas Pfister, and Pradeep Ravikumar. On completeness-aware concept-based explanations in deep neural networks. *Advances in neural information processing systems*, 2019.

[48] Hiroshi Yoshida, Taichi Shimazu, Tomoharu Kiyuna, Atsushi Marugame, Yoshiko Yamashita, Eric Cosatto, Hiroyaku Taniguchi, Shigeki Sekine, and Atsushi Ochiai. Automated histological classification of whole-slide images of gastric biopsy specimens. *Gastric Cancer*, 21(2):249–257, 2018.

[49] Zhendong Zhao, Gang Fu, Sheng Liu, Khaled M Eloky, Robert J Doersken, Yixin Chen, and Dawn E Wilkins. Drug activity prediction using multiple-instance learning via joint instance and feature selection. In *BMC bioinformatics*, volume 14, page S16. Springer, 2013.

Supplementary Materials
ProtoMIL: Multiple Instance Learning with Prototypical
Parts for Fine-Grained Interpretability

In this Supplementary Materials, we present similarity scores visualizations with more instances and prototypes for all datasets considered in our experiments.

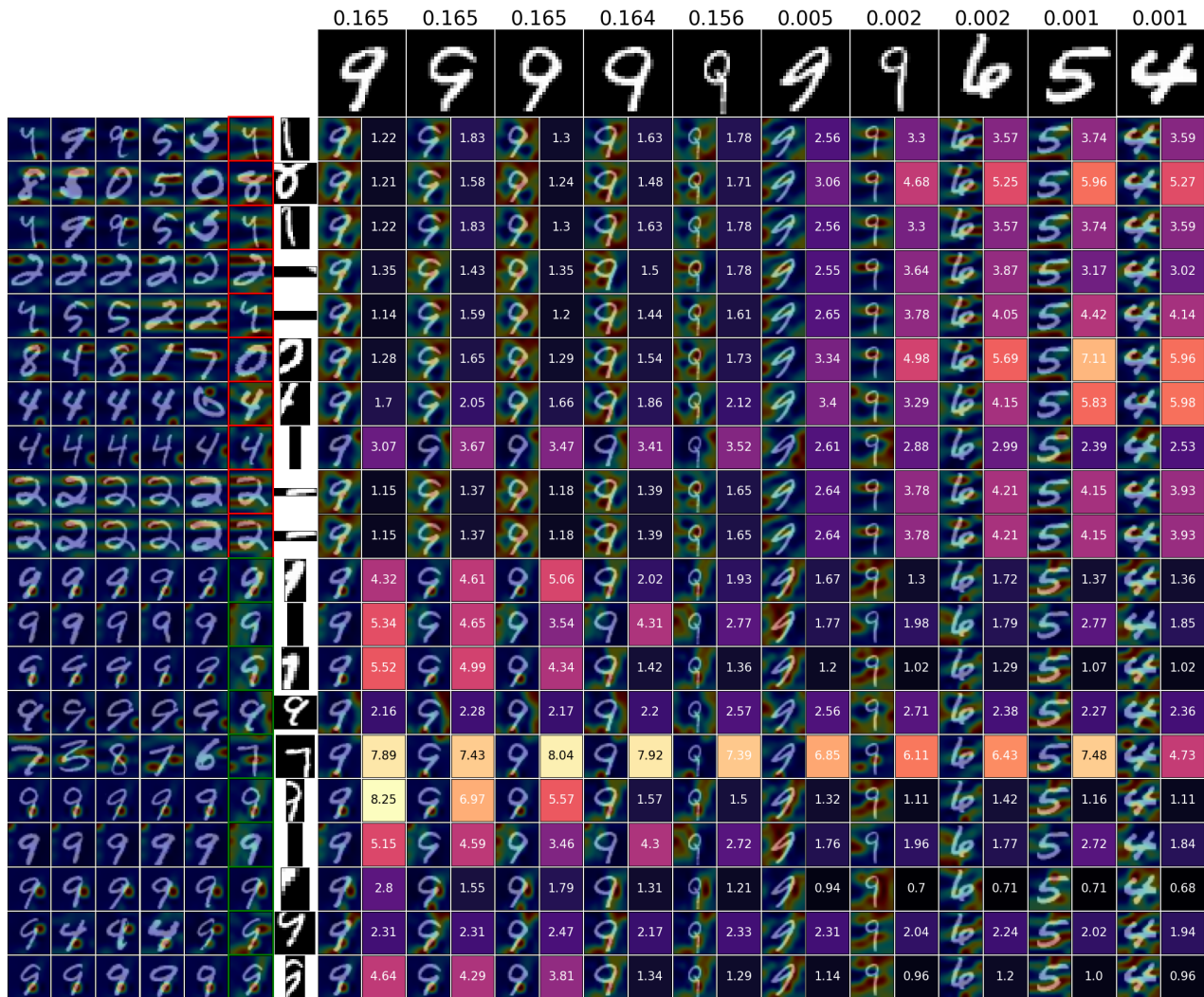


Figure 8: Similarity scores for a positive bag from MNIST Bags.

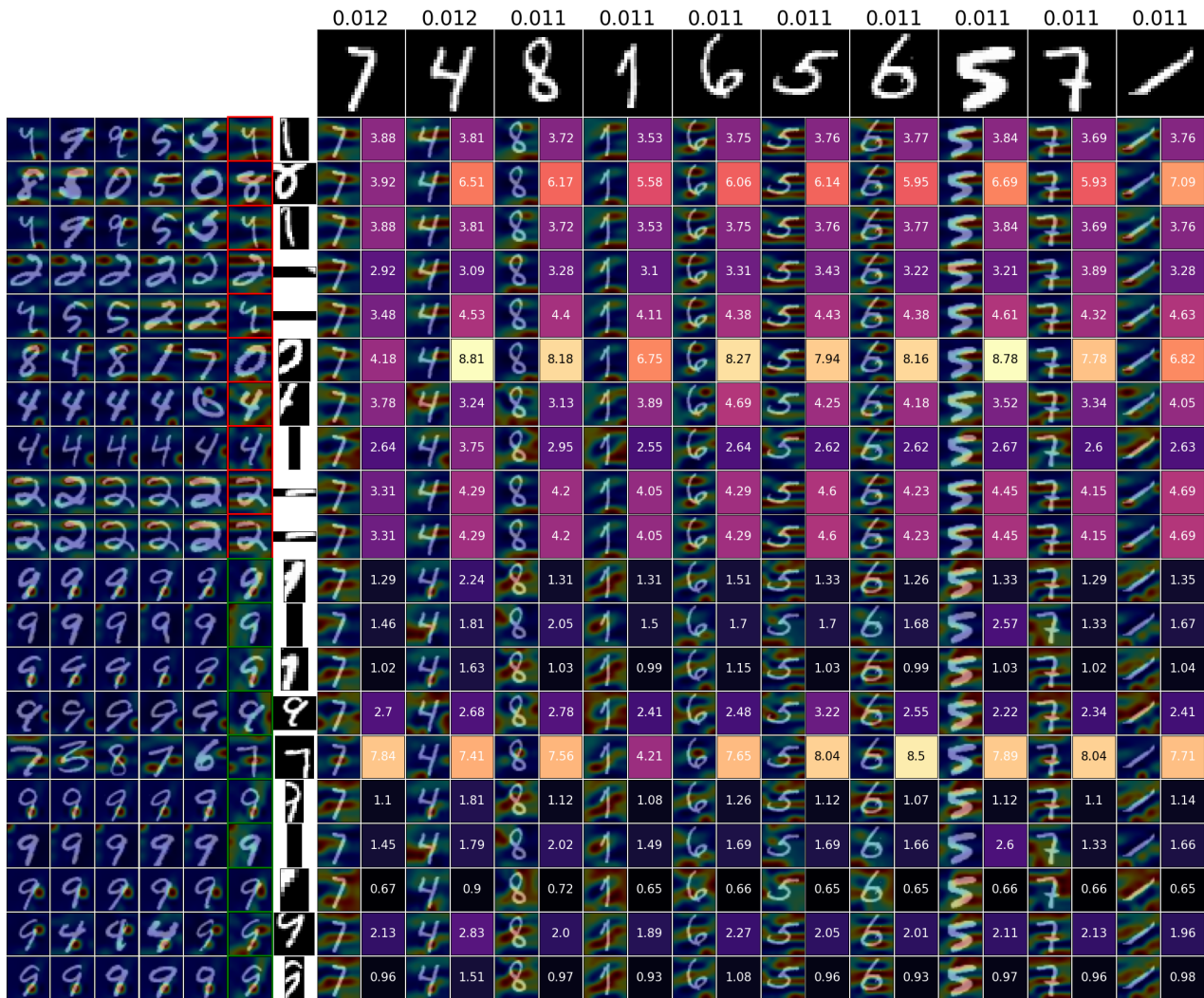


Figure 9: Similarity scores for a negative bag from MNIST Bags.

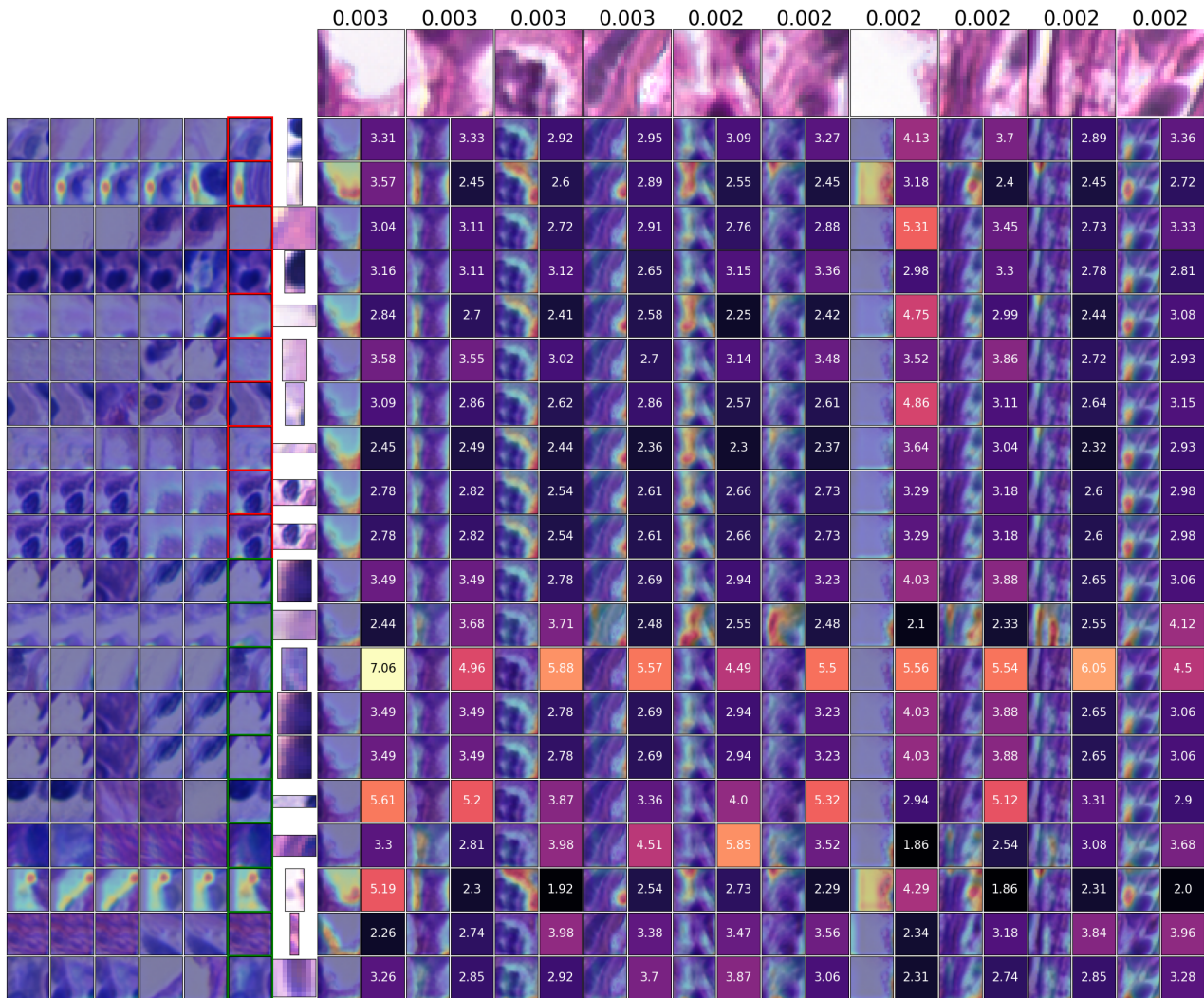


Figure 10: Similarity scores for a positive bag from Bisque dataset.

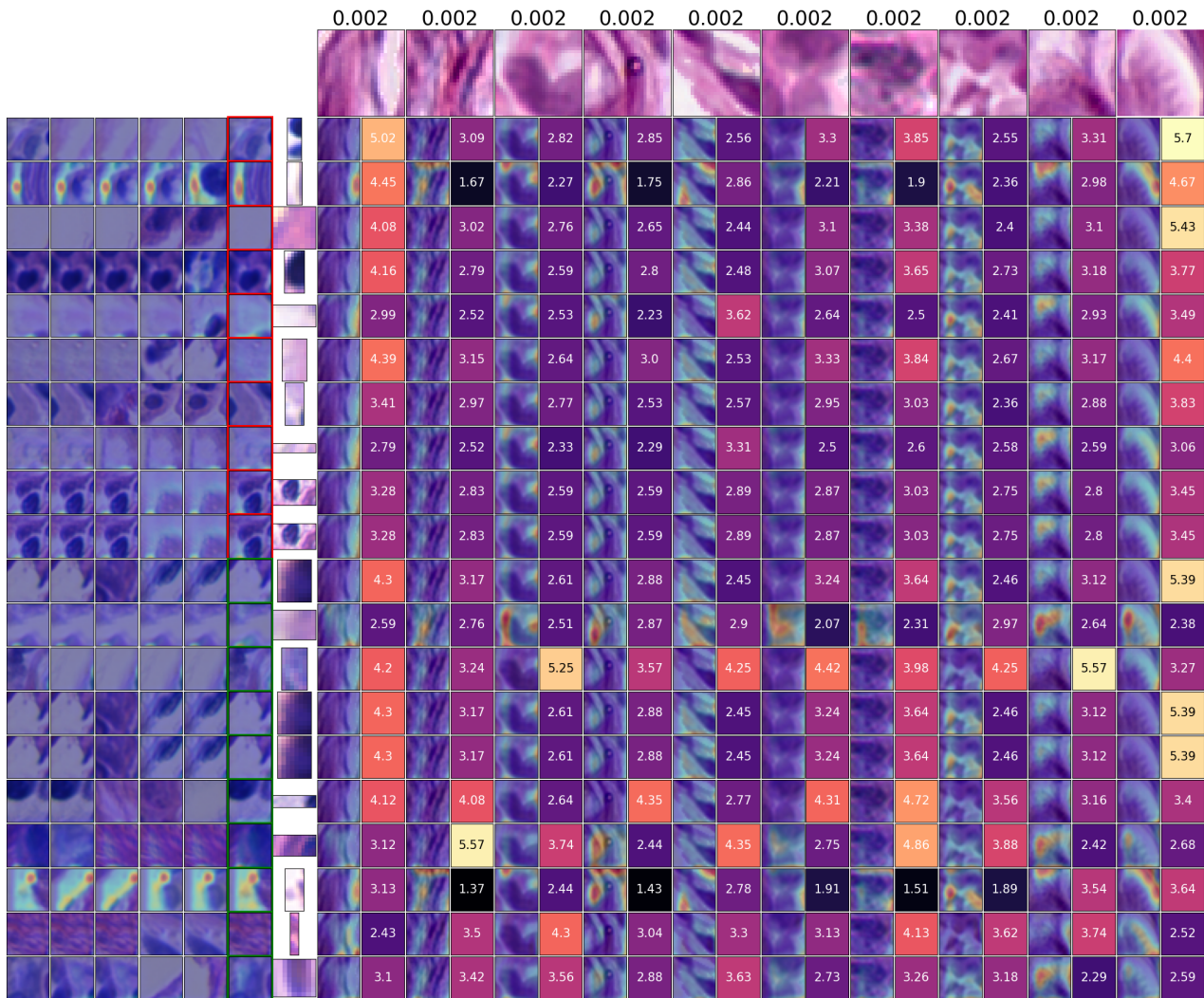


Figure 11: Similarity scores for a negative bag from Bisque dataset.

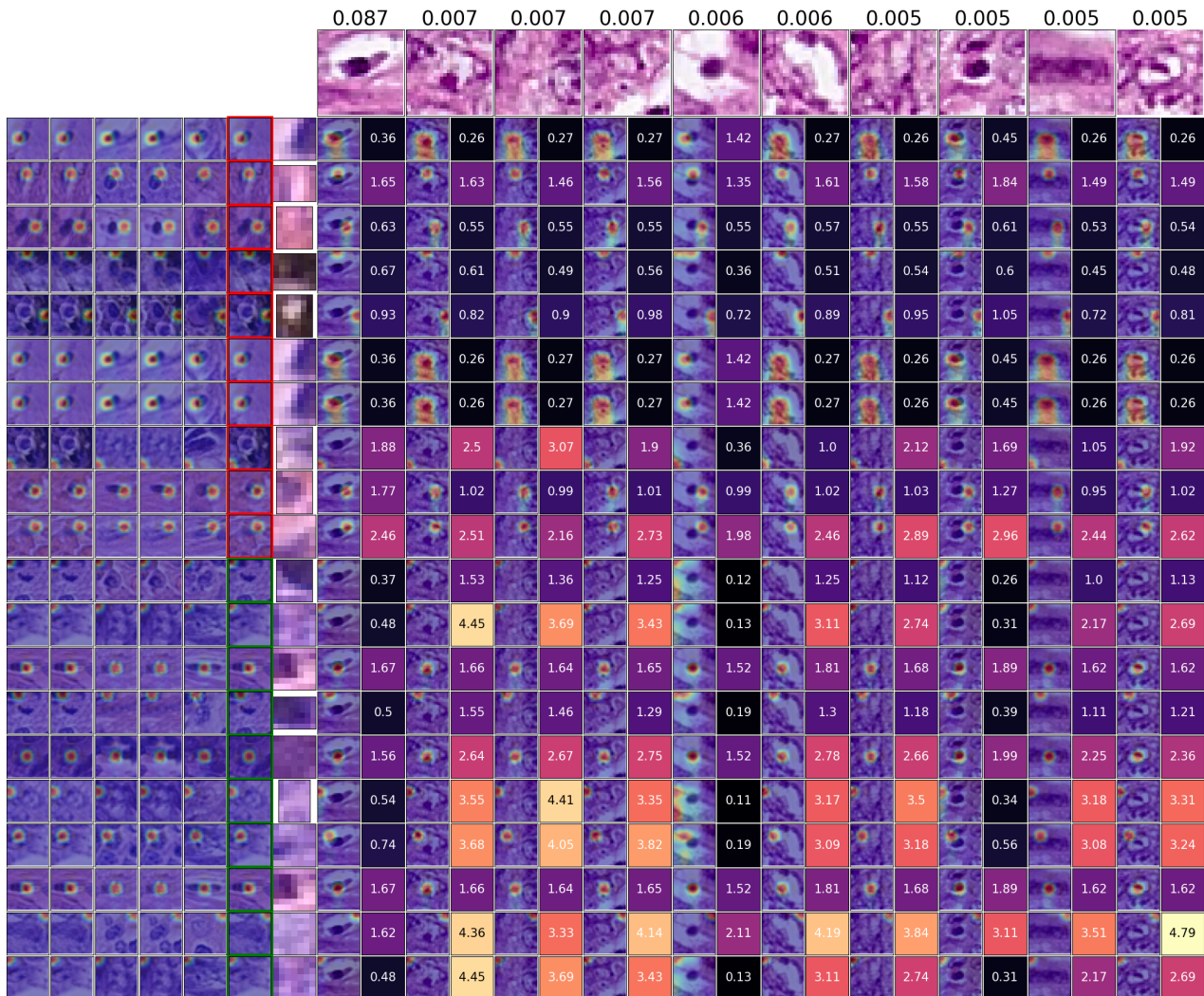


Figure 12: ProtoMIL analysis matrix for a positive example from Colon Cancer dataset.

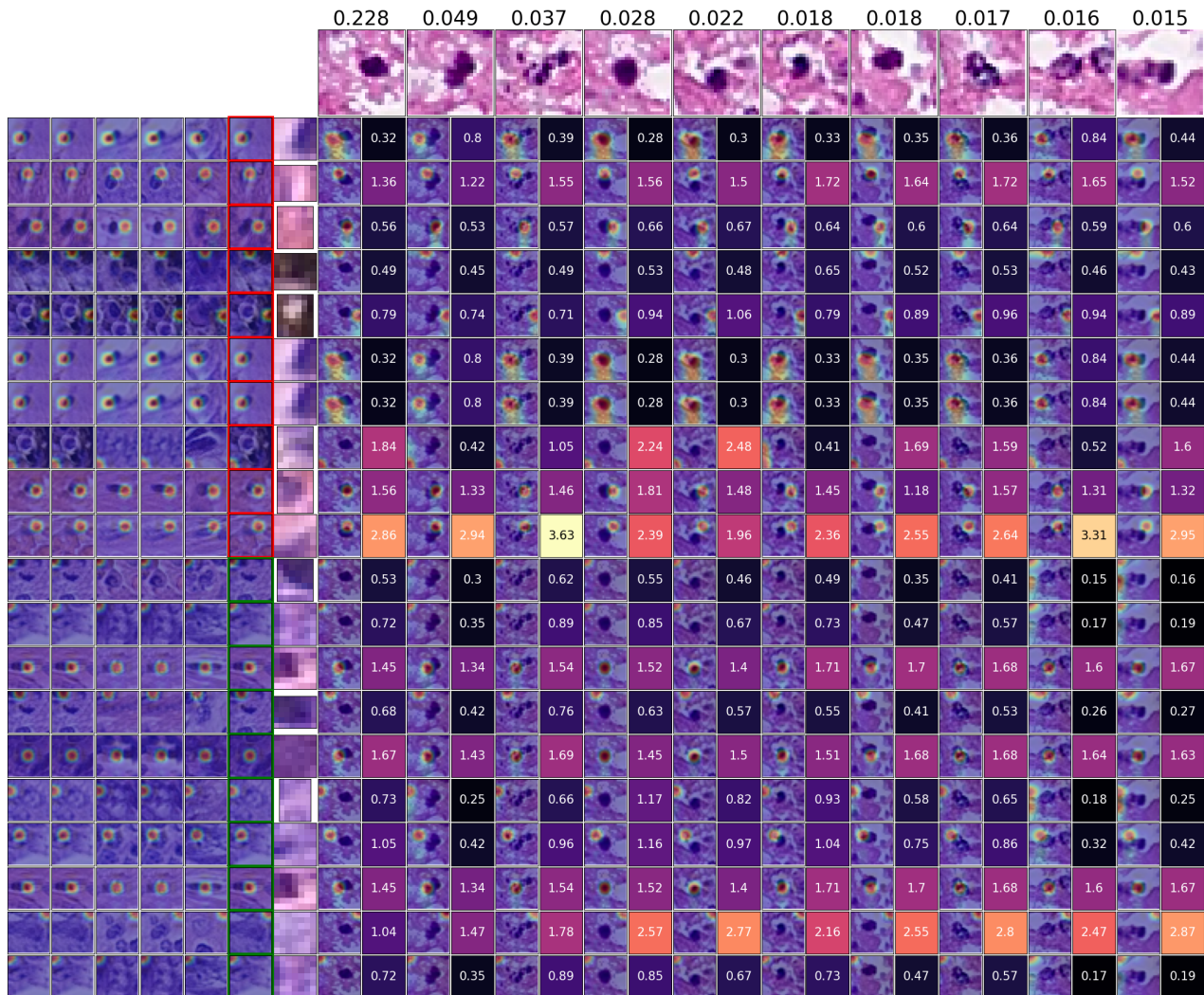


Figure 13: ProtoMIL analysis matrix for a negative example from Colon Cancer dataset.

patches in bag: 31, positive patches: 1, class label: 1

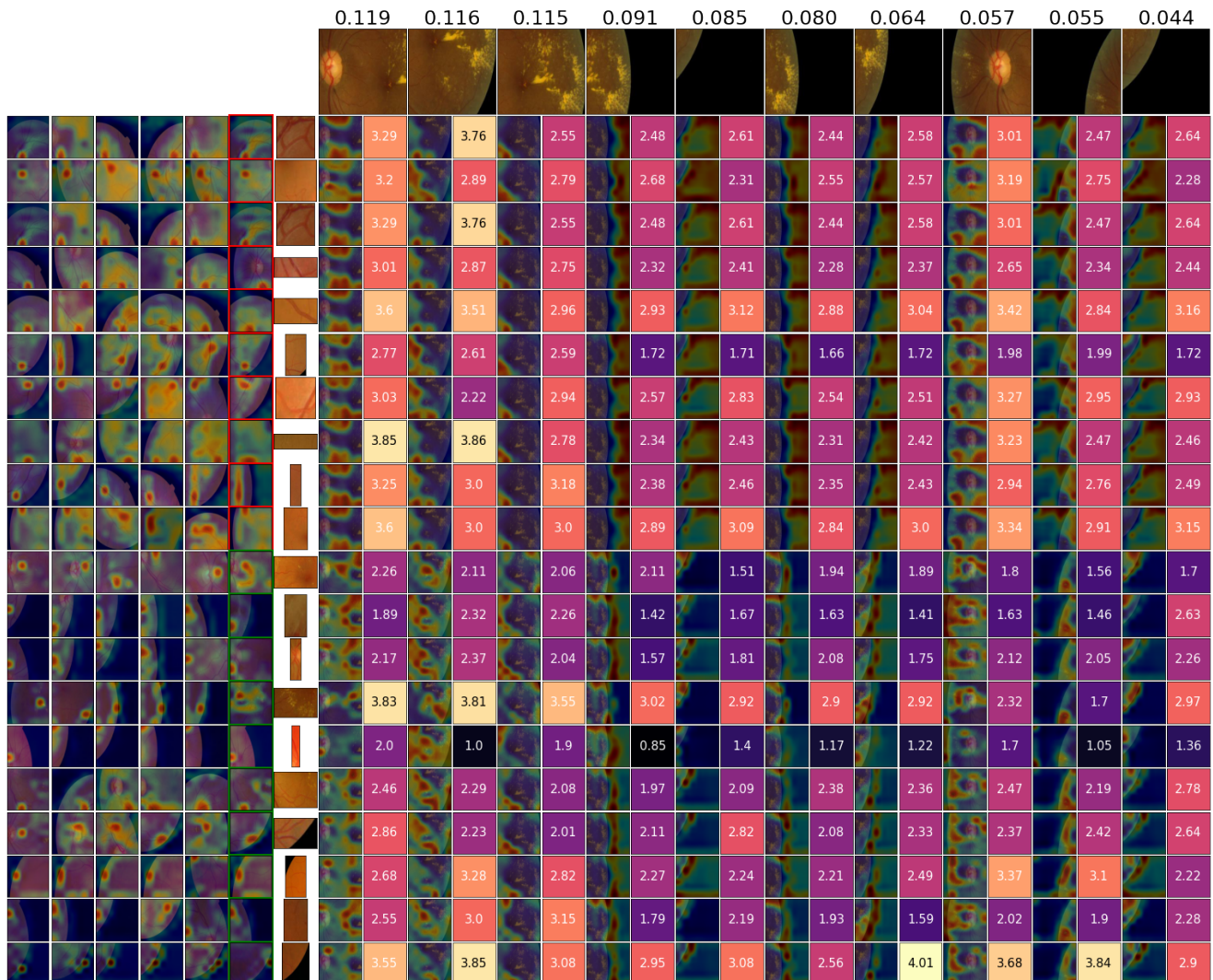


Figure 14: Similarity scores for a positive bag from Messidor dataset.

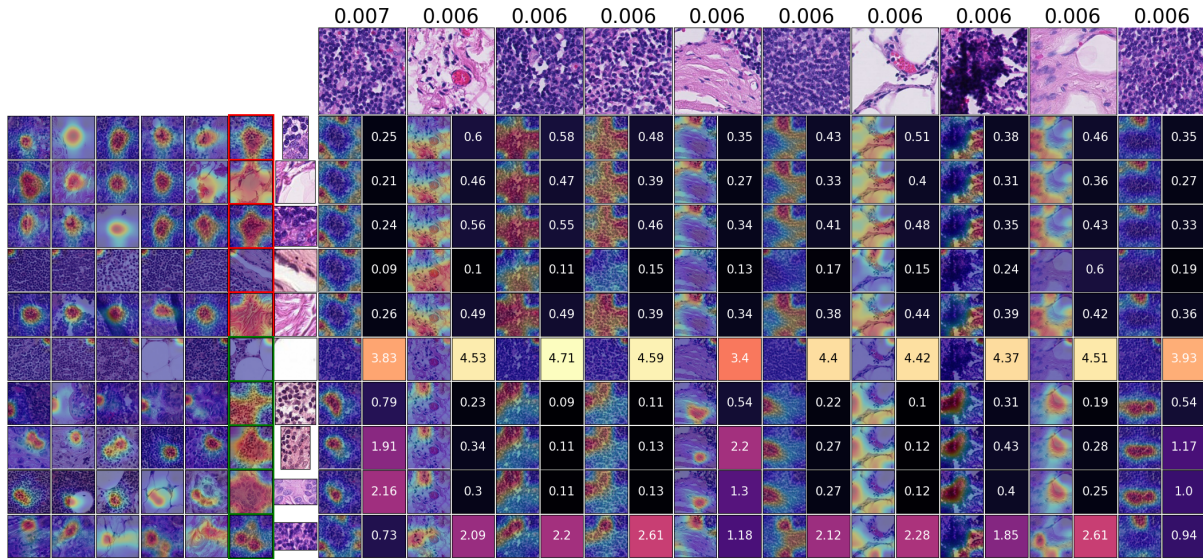


Figure 15: Similarity scores for a positive bag from Camelyon16 dataset.

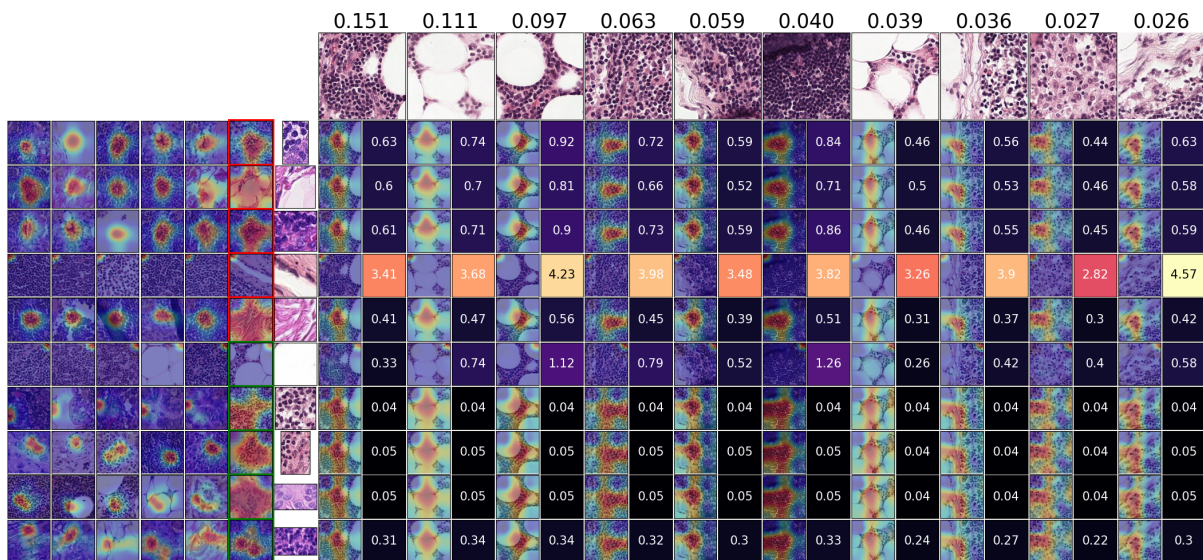


Figure 16: Similarity scores for a negative bag from Camelyon16 dataset.